Energy release rate of the fiber/matrix interface crack in cross-ply $[0^\circ_{m\cdot 2n}, 90^\circ_n]_S$ laminates under transverse loading: debond/bi-material interface interaction

Luca Di Stasio[a,b], Janis Varna[b], Zoubir Ayadi[a]

[a] *Université de Lorraine, EEIGM, IJL, 6 Rue Bastien Lepage, F-54010 Nancy, France*
[b] *Luleå University of Technology, University Campus, SE-97187 Luleå, Sweden*

Abstract

The effects of crack shielding, fiber content and ratio of 0° to 90° ply thickness on fiber/matrix debond growth in thin cross-ply laminates are investigated with Representative Volume Elements (RVEs) of different ordered microstructures. Debond growth is characterized by the estimation of the Energy Release Rates (ERRs) using the Virtual Crack Closure Technique (VCCT) and the J-integral. It is found that

Keywords: Polymer-matrix Composites (PMCs), Thin-ply, Transverse Failure, Debonding, Finite Element Analysis (FEA)

1. Introduction

Since the development of the *spred tow* technology or "FUKUI method" [1, 2], significant efforts have been directed toward the characterization of *thin-ply* laminates [3, 4, 5, 6, 7, 8, 9, 10, 11, 12, 13, 14, 15] and their application to mission-critical structures in the aerospace sector [16, 17, 18, 19].

At the lamina level, the use of *thin-plies* leads to more regular and homogeneous microstructures but no significant imporvement in static properties except for an apparent improvement in compressive strength [12]. Improvements in fatigue life have been observed, although contrasting results can be found in the literature [4, 5, 6]. The beneficial effect of the use of *thin-plies* with respect to damage propagation has been instead commonly observed by different re-

searchers under static [3, 6, 7, 8, 9, 10, 11, 12], fatigue [4, 6, 7, 8, 12] and impact loadings [6, 7, 8, 12]. It seems apparent that *thin-ply* laminates possess an increased ability to delay, and in some cases even suppress, the onset and propagation of transverse cracks (or matrix or micro-cracks).

The first appearance of transverse cracking phenomena is known to be characterized by the appearance of fiber/matrix interface cracks (also referred to as debonds), which grow along the fiber's arc direction, then kink out of the interface and coalesce forming a transverse crack [20]. Different approaches have been applied to model the initiation and growth of debonds. The Cohesive Zone Model (CZM) has been used to mimic the propagation of debonds along fiber interfaces; coupled with a failure criterion for the matrix, it has provided simulations of the growth of transverse cracks starting from a virgin material [21, 22, 23, 24]. The main advantages of this approach are the possibility to observe the development of a simulated crack path and to record a load-displacement curve to compare with experimental measurement. However, various observations cast a doubt about the applicability of the CZM: the bi- (for 2D models) and tri- (in 3D) axiality of the matrix stress state in the inter-fiber region that is linked with a cavitation-like failure of the polymer [25]; the locality and mode dependency of the interface failure [26]; the problematic use at the microscopic level of properties measured in UD specimens at the laminate level [22]. A second approach that obviates these drawbacks is the application of Linear Elastic Fracture Mechanics (LEFM) arguments to the study of debond growth. The analysis focuses on the evaluation of Mode I and Mode II Energy Release Rate (ERR) at the crack tip by means of the Virtual Crack Closure Technique (VCCT) [27] or the J-Integral method [28]. The stress and strain field, required for the ERR computation, can be solved by application of different methodologies such as analytical solutions [29], the Boundary Element Method (BEM) [30] or the Finite Element Method (FEM) [31]. Different works have followed this approach and studied models of one or two fibers in an effectively infinite matrix [32, 33, 34, 35, 36] and of an hexagonal cluster of fibers in an effectively infinite homogenized UD composite [37, 31]. The problem

of debond growth along the fiber-matrix interface in a cross-ply laminate has been only addressed very recently in [38, 39], where the author embed a single partially debonded fiber in an effectively infinite homogenized 90° ply bounded by homogenized 0° layers. Thus, the effect of debond-debond interaction and of the relative proximity of a bi-material interface on the debond's ERR in cross-ply laminates is yet to be addressed. The present work is devoted to this problem. Models of Repeating Unit Cells (RUCs) are developed to represent laminates with different degrees of damage (here only in the form of debonds). The number of fully bonded fibers across the thickness of the 90° ply is varied in order to investigate the effect of the proximity of the bi-material interface. The thickness of the bounding 0° layers is also analyzed as a parameter of the study. The stress and strain fields are solved with the Finite Element Method in Abaqus [40] and the crack characterized by its Mode I and Mode II ERR, calculated with the VCCT and the J-integral method.

2. RVE models & FE discretization

2.1. Introduction & Nomenclature

In the present work, we investigate debond development in cross-ply $[0^\circ_{m\cdot 2n}, 90^\circ_n]_S$ laminates under in-plane transverse tension. The interaction between debonds in the presence of a stiff bi-material interface is studied with the use of different RUCs (see Figures 1 and 2 in Sec. 2.2), in which only the central fiber presents damage in the form of a debond. Repetition of the composite RUC can occur only along the in-plane transverse direction only, thus representing a cross-ply laminate with a thin or even ultra-thin 90° ply in the middle.

The thickness of the 90° ply depends on the number of fibers present across the thickness (the vertical or z direction in Figures 1 and 2) and the value of the fiber volume fraction V_f. On the other hand, the thickness of the 0° layers can be assigned freely as a multiple of the 90° ply thickness, i.e. $t_{0^\circ} = i \cdot t_{90^\circ}$ where i is an arbitrary integer. The thickness ratio i could in theory be assumed to be a real positive number; however, it seems more reasonable to consider it only

as a positive integer based on practical considerations on the actual manufacturing of laminates (stacking of a discrete number of pre-impregnated layers). Thus, the thickness ratio i represents one additional parameter for the investigation. In the RUCs proposed, we consider the 90° ply with debonds as a series of stacked damaged and undamaged fiber rows, each row with only one fiber in the thickness direction. All the RUCs present regular microstructures with fibers placed according to a square-packing configuration and consequently they are Representative Volume Elements (RVE) of cross-ply laminates with a certain distribution of debonds in the middle 90° layer. In the following, let us consider in-plane coordinates x and y, where x is in the transverse direction of the cross-ply laminate under consideration. In the presence of a load in the x-direction, the strain in the y-direction is small, due to the very small minor Poisson's ratio of the laminate. Furthermore, debonds are considered to be significantly longer in the fiber direction than in the arc direction [41]. Therefore we use 2D models under the assumption of plane strain, defined in the $x - z$ section of the composite. The study presented in this paper thus applies to long debonds and its focus ia on understanding the mechanisms of growth along their arc direction. The laminates are assumed to be subject to transverse tensile strain, which is applied in the form of a constant displacement in the x-direction along both vertical boundaries of the RUC as shown in Figure 3.

In summary, the models are differentiated by: first, the spacing between debonds along the horizontal direction in the 90° layer, which corresponds to the number n of fibers in the RUC's horizontal direction; second, the thickness of the middle 90° ply measured in terms of the number k of fiber rows; third, the factor i which provides the thickness of the 0° layers as an integer multiple of the 90° ply thickness. It thus seems natural to introduce the common notation $n \times k - i \cdot t_{90°}$. A final additional model is considered to study the effect of equivalent boundary conditions. This final model is constituted by only one partially debonded fiber. The application of coupling of horizontal displacements in the form of a constant applied displacement along the right and left sides allows for repetition along the horizontal direction. The presence of coupling of vertical displacements and

a linear distribution of horizontal displacements on the bottom and top surfaces models the presence of the stiff bi-material interface between the 90° and the 0° layers. This model is refered to as $1 \times 1 - H + V$ given that: it has respectively 1 fiber in the horizontal and in the vertical direction; on the top and bottom surfaces, both horizontal (H) and vertical (V) displacements are assigned. Finally, two single fiber models similar to $1 \times 1 - H + V$ are considered in the present work for comparison: the $1 \times 1 - free$ and $1 \times 1 - coupling$. In the first, the upper surface is left free; in the second, vertical displacement coupling is applied to the upper boundary. Further details about these models and the corresponding laminate RVE can be found in [42].

2.2. Models of Representative Volume Element (RVE)

The first family of models is represented in Figure 1. It represents a set of $[0^\circ_{m \cdot 2n}, 90^\circ_n]_S$ cross-ply laminates with an ultra-thin 90° layer, constituted by a single row of fibers across the thickness. Debonds appear at regular intervals measured in terms of number n of fully bonded fibers present between them, which in turn correspond to the number of fibers along the horizontal direction of the RUC as highlighted in Fig. 1. They are thus the $n \times 1 - i \cdot t_{90^\circ}$ models, where $i = 1, 10$ and n is an integer ≥ 1 ($n = 1$ corresponds to the case of a debond appearing on all the fibers in the central 90° layer). These models are quite extreme, but allow to focus on the interaction between debonds and the inter-ply bi-material interface. Furthermore, the *spread tow* technology is today capable of producing cross-ply laminates with the central 90° layer thickness only $4 - 5$ times the fiber diameter, as shown for example in [9], which give practical relevance even to such extreme models.

The second set of models considers instead cross-ply laminates with a central 90° ply of variable thickness, measured in terms of number k of fiber rows appearing in the vertical direction in Figure 2. Once again, debonds appear at regular intervals measured in terms of number n of fully bonded fibers present between them, which in turn correspond to the number of fibers along the horizontal direction of the RUC as highlighted in Fig. 2. These models are thus

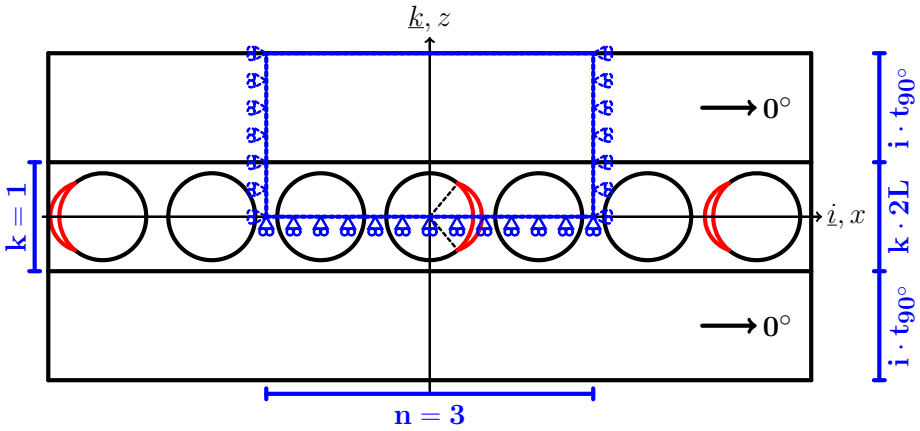

Figure 1: Models of $\left[0^\circ_{m\cdot 2n}, 90^\circ_n\right]_S$ cross-ply laminates with an ultra-thin 90° layer, where the 90° ply is made up by a single "row" of fibers. Debonds are repeating at different distances, measured in terms of the number n of fully bonded fibers appearing between two consecutive debonds.

the $n \times k - i \cdot t_{90^\circ}$ models, where $i = 1, 10$, $k > 1$ and n is an integer ≥ 1 ($n = 1$ corresponds to the case of a debond appearing on all the fibers of the central fiber row in the 90° layer).

By increasing the number n of fibers in the horizontal direction in the RUC, decreasing levels of damage (debonds spaced further apart) are considered to be present in the laminate. By increasing the number k of fiber rows, the thickness of the 90° layer is increased and the effect of the relative proximity of the inter-ply bi-material interface can thus be studied. Finally, by increasing the factor i, the thickness of the 0° layers is increased for a given thickness of the 90°, which allows the investigation of the size effect or *in-situ* effect for the fiber-matrix interface crack.

2.3. Finite Element (FE) discretization

The RUCs are discretized using the Finite Element Method (FEM) with the commercial FEM package Abaqus [40]. The length l and height h of the model are determined by the number of fibers n in the horizontal direction, the number of fiber rows k across the thickness and the thickness ratio i (see

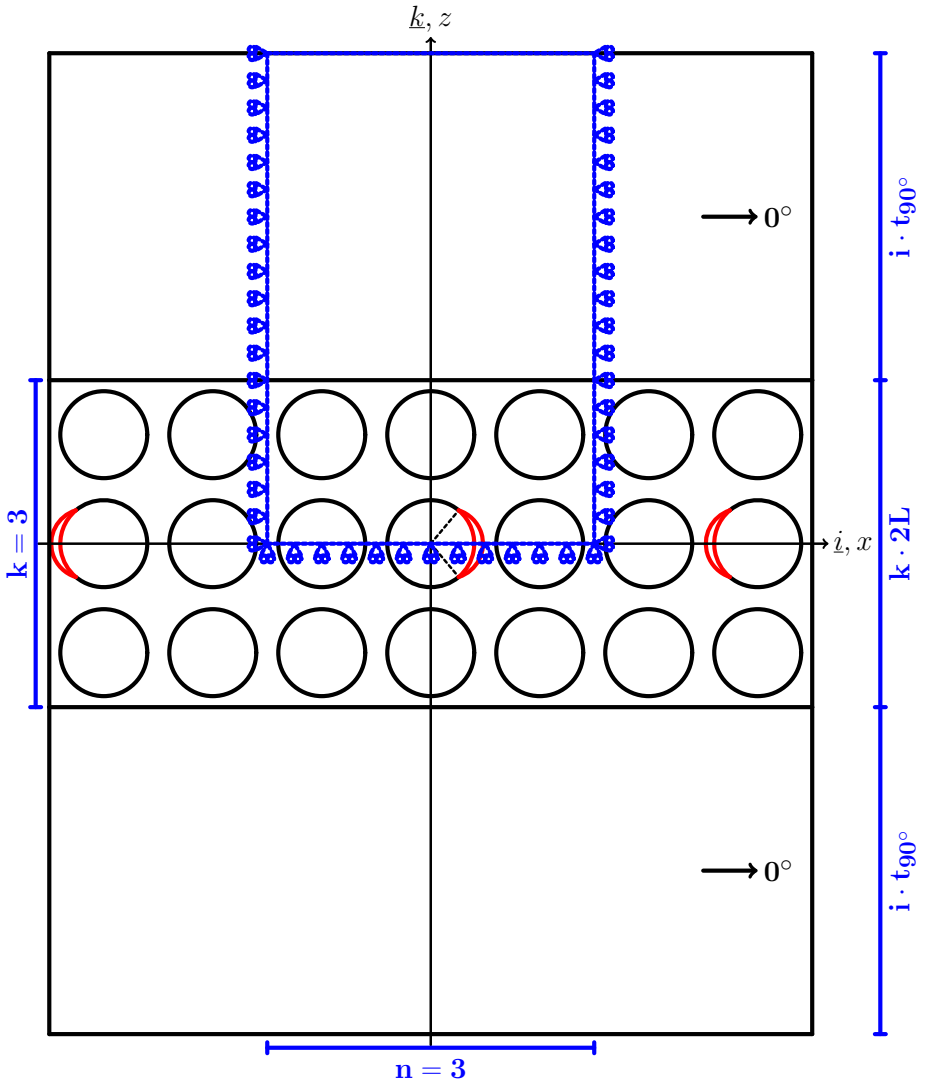

Figure 2: Models of $\left[0^\circ_{m\cdot 2n}, 90^\circ_n\right]_S$ cross-ply laminates with a 90° layer of variable thickness, determined by the number k of "rows" of fibers along the vertical direction. Debonds are repeating at different distances along the horizontal direction, measured in terms of the number n of fully bonded fibers appearing between two consecutive debonds.

Sec. 2.2) according to Eq. 1:

$$l = 2nL \qquad h = (1 + 2i)\, kL. \tag{1}$$

In Eq. 1, $2L$ is the length of a one-fiber unit (see Fig. 3), which in turn is as a function of the fiber volume fraction V_f and the fiber radius according to

$$L = \frac{R_f}{2}\sqrt{\frac{\pi}{V_f}}. \tag{2}$$

Each fiber in the model has the same radius R_f, equal to 1 μm. This specific value has no physical meaning per se and it has been selected for simplicity. It is useful to observe that, in a linear elastic solution as the one described in the present article, the ERR is proportional to the geometrical dimensions of the model and thus re-evaluation of the ERR for fibers of any size requires just a multiplication. Furthermore, the local and global V_f are everywhere equal thanks to the relationships in Eqs. 1 and 2.

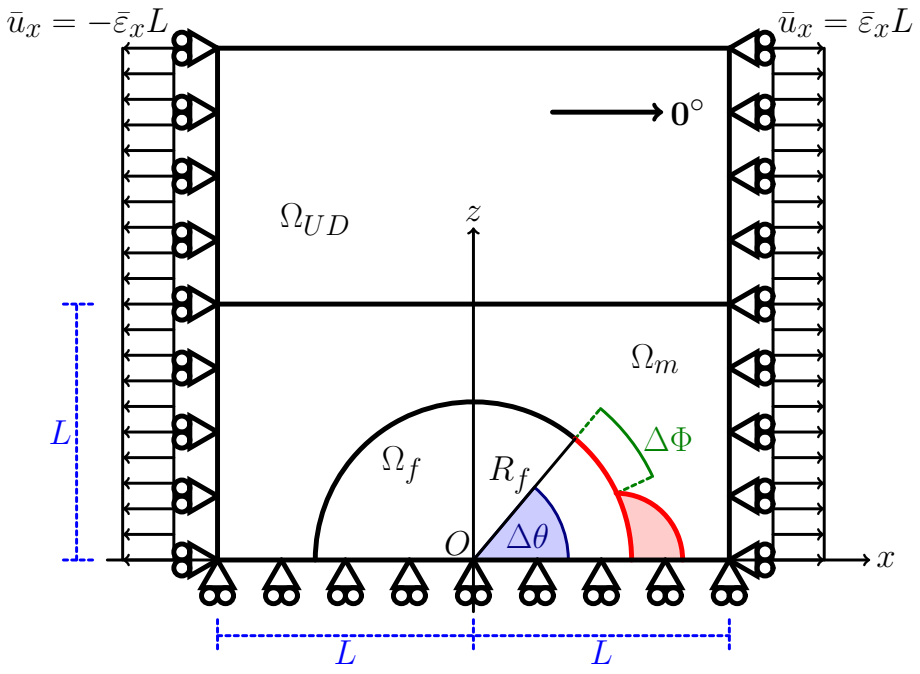

Figure 3: Schematic of the model with its main parameters.

The debond appears symmetrically with respect to the x axis (see Fig. 3) and we characterize it with the angular size $\Delta\theta$ (the full debond size is thus $2\Delta\theta$). In the case of large debond sizes ($\geq 60° - 80°$), a region of size $\Delta\Phi$ to be

determined by the solution itself appears at the crack tip. In this region, called the *contact zone*, the crack faces are in contact and slide on each other. Due to existence of the contact zone, frictionless contact is considered between the two crack faces to avoid interpenetration and allow free sliding. Symmetry with respect to the x axis is applied on the lower boundary. The upper boundary is free, except for the model $1 \times 1 - H + V$ which requires on the upper side kinematic coupling of vertical displacements and applied linearly distributed horizontal displacements. Kinematic coupling on the x-displacement is applied along the left and right boundaries of the model in the form of a constant x-displacement $\pm\bar{\varepsilon}_x l$, corresponding to transverse strain $\bar{\varepsilon}_x$ equal to 1%.

Table 1: Summary of the mechanical properties of fiber, matrix and UD layer. E stands for Young's modulus, μ for shear modulus and ν for Poisson's ratio. Indexes L and T stand respectively for *longitudinal* and *transverse*.

Material	V_f [%]	$E_L\,[GPa]$	$E_T\,[GPa]$	$\mu_{LT}\,[GPa]$	$\nu_{LT}\,[-]$	$\nu_{TT}\,[-]$
Glass fiber	-	70.0	70.0	29.2	0.2	0.2
Epoxy	-	3.5	3.5	1.25	0.4	0.4
UD	60.0	43.442	13.714	4.315	0.273	0.465

The FEM model is discretized using second order, 2D, plane strain triangular (CPE6) and rectangular (CPE8) elements. In the crack tip neighborhood, a refined regular mesh of quadrilateral elements with almost unitary aspect ratio is needed to ensure a correct evaluation of the ERR. The angular size δ of an element in this refined region close to the crack tip is by design equal to 0.05°. The crack faces are modeled as element-based surfaces with a frictionless small-sliding contact pair interaction. The Mode I, Mode II and total Energy Release Rates (ERRs) (respectively G_I, G_{II} and G_{TOT}) represent the main result of the numerical analysis. They are computed using the VCCT [27] implemented in a custom Python routine and the total ERR is obtained from the J-integral [28] evaluation by means of the Abaqus built-in functionality. Glass fiber and epoxy are considered throughout this article, and it is assumed that their response

always lies in the linear elastic domain. The effective UD properties are computed using Hashin's Concentric Cylinder Assembly model [43] with the self-consistency scheme for the out-of-plane shear modulus of Christensen [44]. The properties used are listed in Table 1. The model was validated with respect to BEM results of [45, 35]; considerations about the order of accuracy can be found in [42].

3. Results & Discussion

3.1. Effect of the proximity of the $0°/90°$ *bi-material interface and of the thickness of the* $0°$ *layer on debond ERR*

We first focus our attention on the model $1 \times 1 - i \cdot t_{90°}$, which represents a particular case of the family $n \times k - i \cdot t_{90°}$. It corresponds to a cross-ply laminate in which the central $90°$ ply is constituted by only one fiber row, in which each fiber possesses a debond appearing on alternating sides. The model thus represents an extreme idealization, in the sense that: the central $90°$ layer is the thinniest that can be conceived and cannot actually be produced; second, a very particular damage state is present for which every fiber is partially debonded from the sorrounding matrix. However, the first condition allows us to investigate the direct effect of the proximity of the stiff $0°/90°$ bi-material interface on debond ERR; the second condition prevents the insurgence of strain magnification effects which would be significant in one-fiber-row ply with debonds appearing at regular intervals of fully bonded fibers [42]. The model $1 \times 1 - i \cdot t_{90°}$ thus isolates the effect of the $0°/90°$ bi-material interface. Given that the ratio $i = \frac{t_{0°}}{t_{90°}}$ is a free parameter, we can furthermore study the effect of the thickness of the $0°$ layer on debond ERR.

In Figures 4 and 5 respectively the Mode I and Mode II ERR are compared between models $1 \times 1 - i \cdot t_{90°}$ with $i = 1, 10, 50, 100$ and models $1 \times 1 - free$, $1 \times 1 - coupling$ and $1 \times 1 - H + V$. It is worth to remind us of the laminate RVE that correspond to these last three models: model $1 \times 1 - free$ represents a one-fiber-row UD composite with all the fibers partially debonded; model

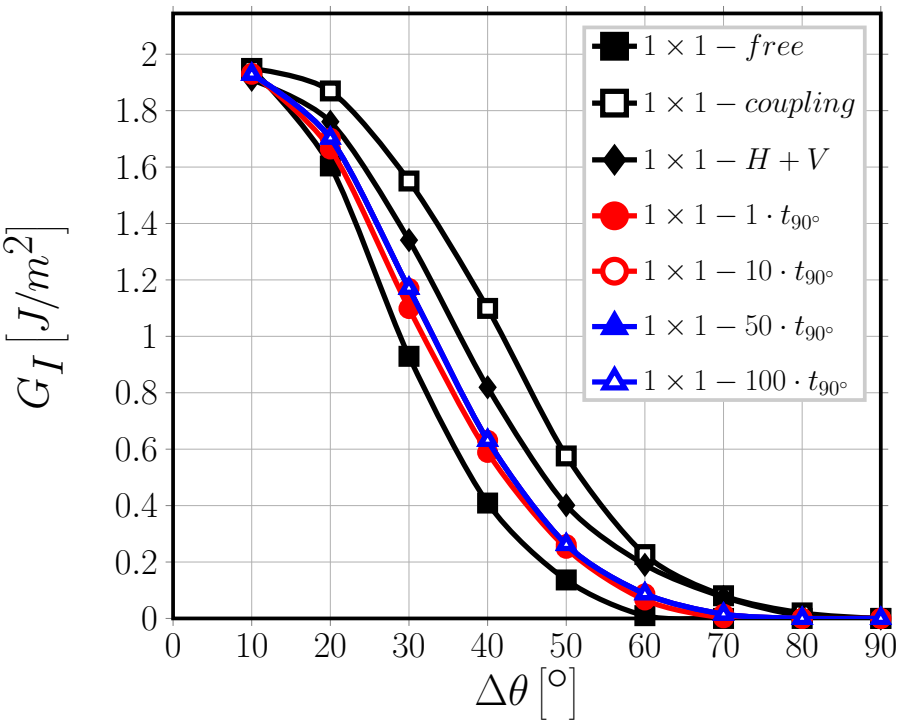

Figure 4: Effect of the proximity of the 0°/90° bi-material interface and of the thickness of the 0° layer on Mode I ERR: models $1 \times 1 - free$, $1 \times 1 - coupling$, $1 \times 1 - H + V$ and $1 \times 1 - i \cdot t_{90°}$. $V_f = 60\%$, $\varepsilon_x = 1\%$.

$1 \times 1 - coupling$ corresponds to a UD laminate with an infinite number of fiber rows and all the fibers partially debonded; model $1 \times 1 - H + V$ represents a cross-ply laminate with one-fiber-row central 90° ply. Observing Figure 4, it is possible to notice that the presence of the 0°/90° bi-material interface translates into a modest increase in the value of G_I with respect to the free surface. For every value of the thickness, however, the values of G_I are lower than those computed with the $1 \times 1 - coupling$ and $1 \times 1 - H + V$ models. A more significant effect can be observed in relation to contact zone onset, which is delayed from $\Delta\theta = 60°$ in the presence of a free surface to 70° in the presence of a homogenized 0° layer. The maximum delay is however reached with the models with equivalent boundary conditions ($1 \times 1 - coupling$ and $1 \times 1 - H + V$),

for which the contact zone onset happens at $\Delta\theta = 80°$. No effect of the thickness of the 0° layer on Mode I ERR can be observed.

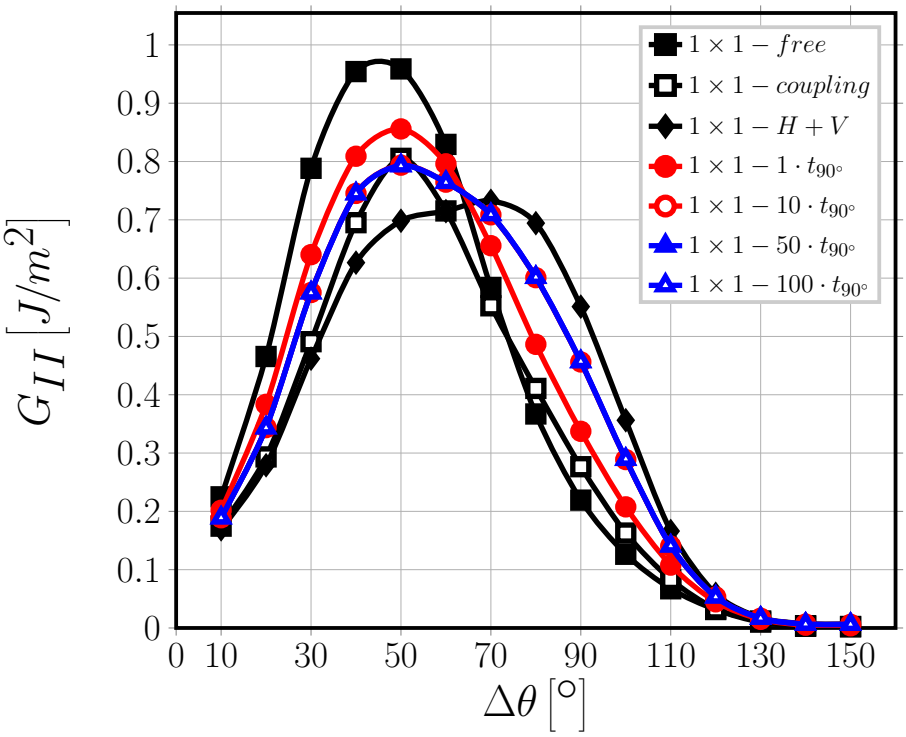

Figure 5: Effect of the proximity of the 0°/90° bi-material interface and of the thickness of the 0° layer on Mode II ERR: models $1\times1-free$, $1\times1-coupling$, $1\times1-H+V$ and $1\times1-i\cdot t_{90°}$. $V_f = 60\%$, $\varepsilon_x = 1\%$.

The presence of the 0°/90° bi-material interface causes instead a decrease of Mode II for open debonds ($\Delta\theta < 60° - 70°$) and a decrease for close debonds ($\Delta\theta > 60° - 70°$) with respect to the free surface case (see Fig. 5). The trend is the same as the one of the model $1\times1-H+V$, but more modest in magnitude. A small effect of the thickness of the 0° layer on Mode II ERR can be noticed in Fig. 5 when the ratio $i = \frac{t_{0°}}{t_{90°}}$ is increased from 1 to 10. The change between the two follows the same pattern described previously: when the thickness of the 0° ply is increased, Mode II decreases for open debonds and increases for closed debonds.

These results help to shed light on the effect of the $0°/90°$ bi-material interface on debond ERR. The presence of the stiff homogenized $0°$ layer causes the matrix placed relatively far from the fiber (close to the left and right sides) to contract much less than it would do in the presence of a free surface due to its relatively high Poisson's ratio. Furthermore, the presence of the $0°/90°$ bi-material interface induces a more homogeneous x-displacement field all over the matrix domain. This causes a concurrent increase of G_I and decrease of G_{II} for small debonds, where the crack opening displacement component at the crack tip (responsible for Mode I) is mostly due to the global x-displacement field (which increase in the presence of the $0°/90°$ bi-material interface) while the crack shear displacement component at the crack tip (responsible for Mode II) is instead linked to the global vertical displacement field due to Poisson's effect (which is decreasing). This causes also the delay in the onset of the contact zone. For large debonds instead, after the onset of the contact zone, the situation reverses: the magnitude increase of the global x-displacement field leads to an increase in the crack shear displacement component at the crack tip and thus in Mode II ERR. By comparing the results for Mode II of models $1 \times 1 - free$, $1 \times 1 - H + V$ and $1 \times 1 - i \cdot t_{90°}$ with $i = 1, 10, 50, 100$ (Fig. 5), it can be argued that the effect of the $0°$ ply thickness is related to the distance of the free surface: for $t_{0°} = t_{90°}$ a modest effect of the presence of the upper free surface of the $0°$ ply is still felt by the debond and the effect of the $0°/90°$ bi-material interface previously described is reduced, with the ERR values closer to the $1 \times 1 - free$ model. When the thickness ratio is increased to 10, the effect disappears. No further change is observed for thicker $0°$ layers.

3.2. Effect of the proximity of the $0°/90°$ *bi-material interface on debond-debond interaction in a single fiber row* $90°$ *ply*

3.3. Interaction between layers of fully bonded fibers and a centrally located line of debonded fibers in a $90°$ *ply inside a* $[0°_n, 90°]_S$ *laminate*

3.4. Interaction of debonds within a $90°$ *ply with multiple layers of fibers inside a* $[0°_n, 90°]_S$ *laminate*

4. Conclusions & Outlook

Acknowledgements

Luca Di Stasio gratefully acknowledges the support of the European School of Materials (EUSMAT) through the DocMASE Doctoral Programme and the European Commission through the Erasmus Mundus Programme.

References

[1] K. Kawabe, New spreading technology for carbon fiber tow and its application to composite materials, Sen'i Gakkaishi 64 (8) (2008) 262–267. doi:10.2115/fiber.64.p_262.

[2] K. Kawabe, H. Sasayama, S. Tomoda, New carbon fiber tow-spread technology and applications to advanced composite materials, SAMPE Journal 45 (2) (2008) 6–17.

[3] H. Sasayama, K. Kawabe, S. Tomoda, I. Ohsawa, K. Kageyama, N. Ogata, Effect of lamina thickness on first ply failure in multidirectionally laminated composites, in: Proceedings of the 8^{th} Japan SAMPE Symposium, SAMPE, 2003.

[4] K. Yamaguchi, H. Hahn, The improved ply cracking resistance of thin-ply laminates, in: Proceedings of the 15^{th} International Conference on Composite Materials (ICCM-15), SAMPE, 2005.

[5] S. Tsai, S. Sihn, R. Kim, Thin ply composites, in: Proceedings of 46^{th} AIAA/ASME/AHS/ASC Structures, Structural Dynamics & Materials Conference, 2005.

[6] S. Sihn, R. Kim, K. Kawabe, S. Tsai, Experimental studies of thin-ply laminated composites, Composites Science and Technology 67 (6) (2007) 996–1008. doi:10.1016/j.compscitech.2006.06.008.

[7] T. Yokozeki, Y. Aoki, T. Ogasawara, Experimental characterization of strength and damage resistance properties of thin-ply carbon fiber/toughened epoxy laminates, Composite Structures 82 (3) (2008) 382–389. doi:10.1016/j.compstruct.2007.01.015.

[8] T. Yokozeki, A. Kuroda, A. Yoshimura, T. Ogasawara, T. Aoki, Damage characterization in thin-ply composite laminates under out-of-plane transverse loadings, Composite Structures 93 (1) (2010) 49–57. doi:10.1016/j.compstruct.2010.06.016.

[9] H. Saito, H. Takeuchi, I. Kimpara, Experimental evaluation of the damage growth restraining in 90 layer of thin-ply cfrp cross-ply laminates, Advanced Composite Materials 21 (1) (2012) 57–66. doi:10.1163/156855112X629522.

[10] A. Arteiro, G. Catalanotti, J. Xavier, P. Camanho, Notched response of non-crimp fabric thin-ply laminates, Composites Science and Technology 79 (2013) 97–114. doi:10.1016/j.compscitech.2013.02.001.

[11] A. Arteiro, G. Catalanotti, J. Xavier, P. Camanho, Large damage capability of non-crimp fabric thin-ply laminates, Composites Part A: Applied Science and Manufacturing 63 (2014) 110–122. doi:10.1016/j.compositesa.2014.04.002.

[12] R. Amacher, J. Cugnoni, J. Botsis, L. Sorensen, W. Smith, C. Dransfeld, Thin ply composites: Experimental characterization and modeling of size-

effects, Composites Science and Technology 101 (2014) 121–132. doi:10.1016/j.compscitech.2014.06.027.

[13] G. Guillamet, A. Turon, J. Costa, J. Renart, P. Linde, J. Mayugo, Damage occurrence at edges of non-crimp-fabric thin-ply laminates under off-axis uniaxial loading, Composites Science and Technology 98 (2014) 44–50. doi:10.1016/j.compscitech.2014.04.014.

[14] C. Huang, S. Ju, M. He, Q. Zheng, Y. He, J. Xiao, J. Zhang, D. Jiang, Identification of failure modes of composite thin-ply laminates containing circular hole under tension by acoustic emission signals, Composite Structures 206 (2018) 70–79. doi:10.1016/j.compstruct.2018.08.019.

[15] J. Cugnoni, R. Amacher, S. Kohler, J. Brunner, E. Kramer, C. Dransfeld, W. Smith, K. Scobbie, L. Sorensen, J. Botsis, Towards aerospace grade thin-ply composites: Effect of ply thickness, fibre, matrix and interlayer toughening on strength and damage tolerance, Composites Science and Technology 168 (2018) 467–477. doi:10.1016/j.compscitech.2018.08.037.

[16] J.-B. Moon, M.-G. Kim, C.-G. Kim, S. Bhowmik, Improvement of tensile properties of CFRP composites under LEO space environment by applying MWNTs and thin-ply, Composites Part A: Applied Science and Manufacturing 42 (6) (2011) 694–701. doi:10.1016/j.compositesa.2011.02.011.

[17] Y. H. N. Kim, S. Ko, W.-S. Lay, J. Tian, P. Chang, S. U. Thielk, H.-J. Bang, J. Yang, Effects of shallow biangle, thin-ply laminates on structural performance of composite wings, AIAA Journal 55 (6) (2017) 2086–2092. doi:10.2514/1.j055465.

[18] A. Kopp, S. Stappert, D. Mattsson, K. Olofsson, E. Marklund, G. Kurth, E. Mooij, E. Roorda, The aurora space launcher concept, CEAS Space Journal 10 (2) (2017) 167–187. doi:10.1007/s12567-017-0184-2.

[19] D. A. McCarville, J. C. Guzman, A. K. Dillon, J. R. Jackson, J. O. Birkland, 3.5 Design, Manufacture and Test of Cryotank Components, Elsevier, 2018, pp. 153–179. doi:10.1016/b978-0-12-803581-8.09958-6.

[20] J. E. Bailey, A. Parvizi, On fibre debonding effects and the mechanism of transverse-ply failure in cross-ply laminates of glass fibre/thermoset composites, Journal of Materials Science 16 (3) (1981) 649–659. doi:10.1007/bf02402782.

[21] V. Kushch, S. Shmegera, P. Brøndsted, L. Mishnaevsky, Numerical simulation of progressive debonding in fiber reinforced composite under transverse loading, International Journal of Engineering Science 49 (1) (2011) 17–29. doi:10.1016/j.ijengsci.2010.06.020.

[22] L. P. Canal, C. González, J. Segurado, J. LLorca, Intraply fracture of fiber-reinforced composites: Microscopic mechanisms and modeling, Composites Science and Technology 72 (11) (2012) 1223–1232. doi:10.1016/j.compscitech.2012.04.008.

[23] L. Bouhala, A. Makradi, S. Belouettar, H. Kiefer-Kamal, P. Fréres, Modelling of failure in long fibres reinforced composites by x-FEM and cohesive zone model, Composites Part B: Engineering 55 (2013) 352–361. doi:10.1016/j.compositesb.2012.12.013.

[24] M. Herráez, D. Mora, F. Naya, C. S. Lopes, C. González, J. LLorca, Transverse cracking of cross-ply laminates: A computational micromechanics perspective, Composites Science and Technology 110 (2015) 196–204. doi:10.1016/j.compscitech.2015.02.008.

[25] L. E. Asp, L. A. Berglund, P. Gudmundson, Effects of a composite-like stress state on the fracture of epoxies, Composites Science and Technology 53 (1) (1995) 27–37. doi:10.1016/0266-3538(94)00075-1.

[26] V. Mantič, Interface crack onset at a circular cylindrical inclusion under a remote transverse tension. application of a coupled stress and energy

criterion, International Journal of Solids and Structures 46 (6) (2009) 1287–1304. doi:10.1016/j.ijsolstr.2008.10.036.

[27] R. Krueger, Virtual crack closure technique: History, approach, and applications, Applied Mechanics Reviews 57 (2) (2004) 109. doi:10.1115/1.1595677.

[28] J. R. Rice, A path independent integral and the approximate analysis of strain concentration by notches and cracks, Journal of Applied Mechanics 35 (2) (1968) 379. doi:10.1115/1.3601206.

[29] M. Toya, A crack along the interface of a circular inclusion embedded in an infinite solid, Journal of the Mechanics and Physics of Solids 22 (5) (1974) 325–348. doi:10.1016/0022-5096(74)90002-7.

[30] F. París, J. C. Caño, J. Varna, The fiber-matrix interface crack — a numerical analysis using boundary elements, International Journal of Fracture 82 (1) (1996) 11–29. doi:10.1007/bf00017861.

[31] L. Zhuang, A. Pupurs, J. Varna, R. Talreja, Z. Ayadi, Effects of inter-fiber spacing on fiber-matrix debond crack growth in unidirectional composites under transverse loading, Composites Part A: Applied Science and Manufacturing 109 (2018) 463–471. doi:10.1016/j.compositesa.2018.03.031.

[32] E. Correa, V. Mantič, F. París, Effect of thermal residual stresses on matrix failure under transverse tension at micromechanical level: A numerical and experimental analysis, Composites Science and Technology 71 (5) (2011) 622–629. doi:10.1016/j.compscitech.2010.12.027.

[33] E. Correa, F. París, V. Mantič, Effect of the presence of a secondary transverse load on the inter-fibre failure under tension, Engineering Fracture Mechanics 103 (2013) 174–189. doi:10.1016/j.engfracmech.2013.02.026.

[34] E. Correa, F. París, V. Mantič, Effect of a secondary transverse load on the inter-fibre failure under compression, Composites Part B: Engineering 65 (2014) 57–68. doi:10.1016/j.compositesb.2014.01.005.

[35] C. Sandino, E. Correa, F. París, Numerical analysis of the influence of a nearby fibre on the interface crack growth in composites under transverse tensile load, Engineering Fracture Mechanics 168 (2016) 58–75. doi:10.1016/j.engfracmech.2016.01.022.

[36] C. Sandino, E. Correa, F. París, Interface crack growth under transverse compression: nearby fibre effect, in: Proceeding of the 18^{th} European Conference on Composite Materials (ECCM-18), 2018.

[37] J. Varna, L. Q. Zhuang, A. Pupurs, Z. Ayadi, Growth and interaction of debonds in local clusters of fibers in unidirectional composites during transverse loading, Key Engineering Materials 754 (2017) 63–66. doi:10.4028/www.scientific.net/kem.754.63.

[38] M. Velasco, E. Graciani, L. Távara, E. Correa, F. París, BEM multiscale modelling involving micromechanical damage in fibrous composites, Engineering Analysis with Boundary Elements 93 (2018) 1–9. doi:10.1016/j.enganabound.2018.03.012.

[39] F. París, M. L. Velasco, E. Correa, Micromechanical study on the influence of scale effect in the first stage of damage in composites, Composites Science and Technology 160 (2018) 1–8. doi:10.1016/j.compscitech.2018.03.004.

[40] Simulia, Providence, RI, USA, ABAQUS/Standard User's Manual, Version 6.12 (2012).

[41] H. Zhang, M. Ericson, J. Varna, L. Berglund, Transverse single-fibre test for interfacial debonding in composites: 1. experimental observations, Composites Part A: Applied Science and Manufacturing 28 (4) (1997) 309–315. doi:10.1016/s1359-835x(96)00123-6.

[42] L. D. Stasio, J. Varna, Z. Ayadi, Energy release rate of the fiber/matrix interface crack in ud composites under transverse loading: debond-debond and debond-free boundary interactions, submitted to Theoretical and Applied Fracture Mechanics.

[43] Z. Hashin, Analysis of composite materials—a survey, Journal of Applied Mechanics 50 (3) (1983) 481. doi:10.1115/1.3167081.

[44] R. Christensen, K. Lo, Solutions for effective shear properties in three phase sphere and cylinder models, Journal of the Mechanics and Physics of Solids 27 (4) (1979) 315–330. doi:10.1016/0022-5096(79)90032-2.

[45] F. París, E. Correa, V. Mantič, Kinking of transversal interface cracks between fiber and matrix, Journal of Applied Mechanics 74 (4) (2007) 703. doi:10.1115/1.2711220.